Mon. Not. R. astr. Soc. (1987) **228**, 557–571

Rotation measure variation across M84

Robert A. Laing *Royal Greenwich Observatory, Herstmonceux Castle, Hailsham, East Sussex BN27 1RP*

Alan H. Bridle *National Radio Astronomy Observatory,* Edgemont Road, Charlottesville, Virginia 22903-2475, USA*

Accepted 1987 April 6. Received 1987 April 6; in original form 1987 March 4

Summary. VLA images of the linearly polarized emission from the weak radio galaxy M84 (3C272.1) with 3.9 arcsec resolution at 1.4 and 4.9 GHz show an organized pattern of Faraday rotation measure across the radio source. This pattern implies that there is a magnetoionic medium ~10 kpc in extent within M84, in front of, but not mixed with, the radio-emitting plasma. There must be a large-scale reversal in the magnetic field in this medium across the face of the radio source. The medium may be responsible for the more diffuse component of the X-ray emission from M84, and there is evidence that it is interacting with the outflow in the two radio jets.

1 Introduction

Studies of the effects of Faraday rotation on the polarized radio emission from extragalactic sources provide information about the distributions of ordered magnetic fields and ionized gas both within and in front of them (e.g. Burn 1966; Laing 1985). Indeed, it is difficult to determine the magnetic field configurations in the interstellar media of elliptical galaxies by any other means. Observations of the (weak) radio galaxies NGC 6251 by Perley, Bridle & Willis (1984), 3C 449 by Cornwell & Perley (1985) and NGC 1265 by O'Dea & Owen (1986) have shown that most of the Faraday rotation affecting these sources is produced by foreground material, some of which must be associated with the sources themselves, the remainder being in our Galaxy. These observations sample the distribution of Faraday rotation only along narrow radio jets. To obtain more information about the two-dimensional distributions of ionized gas and magnetic fields in radio galaxies, we must study sources that have extended, two-dimensional radio structures. It is particularly interesting to study wide-lobed radio structures that are associated with galaxies for which there are also optical and X-ray data on the distributions of ionized material.

This paper reports observations of the distribution of Faraday rotation measure over such a radio source – 3C 272.1, identified with M84 (NGC 4374), a prominent elliptical galaxy in the core

*The NRAO is operated by Associated Universities, Inc., under contract with The National Science Foundation.

of the Virgo Cluster. This radio source is about 3 arcmin (13 kpc) in extent, and has a monochromatic power at 1.4 GHz of $P_{1.4}=1.9\times10^{23}\,\mathrm{W\,Hz^{-1}}$ (assuming M84 to be at the distance $d=15.7$ Mpc derived for the Virgo Cluster by Mould, Aaronson & Huchra 1980). The inner ~20 arcsec (1.5 kpc) of the galaxy exhibits LINER-like optical emission lines of Hα, [O II], [N II] and [S II] (Hansen, Nørgaard-Nielsen & Jørgensen 1985), and is crossed by a dust lane approximately at right angles to the innermost radio structure (Wade 1960; Kotanyi & Ekers 1979; Hansen *et al.* 1985). There is also a soft X-ray source ~90 arcsec (7 kpc) in extent around the nucleus with a 0.5–3 keV luminosity of $3\times10^{40}\,\mathrm{erg\,s^{-1}}$, converting the value derived by Forman, Jones & Tucker (1984, 1985) to $d=15.7$ Mpc. The X-ray source has been interpreted as thermal bremsstrahlung emission from an interstellar medium in M84 at a temperature $T\approx10^7$ K whose density distribution can be approximated by a King model with a central electron density of $n_e\approx10^{-1}\,\mathrm{cm^{-3}}$ and a core radius $a\approx2$ kpc (Forman & Jones 1982; Forman *et al.* 1985). The source is also embedded in the intracluster medium of the Virgo Cluster, which, at the 400 kpc distance of M84 from the cluster centre, has $n_e\sim2$–$3\times10^{-4}\,\mathrm{cm^{-3}}$ and $T\sim2$–3×10^7 K (Stewart *et al.* 1984 and references therein).

2 Observations

We observed the radio source with the VLA in its *A*, *B* and *C* configurations at 1.413 and 4.885 GHz as shown in Table 1. The flux density scales of the observations were normalized to that of Baars *et al.* (1977) by observing 3C 286, whose flux density on this scale is 14.77 Jy at 1.413 GHz and 7.41 Jy at 4.885 GHz. The flux density normalization is believed to be accurate to ±2 per cent at both frequencies. The phases were initially calibrated by interpolation from observations of the unresolved calibrators 1236+077 (*A* configuration) and 1252+119 (*B* and *C* configurations). The observations of these sources were also used to determine the on-axis instrumental cross-polarization properties. The zero point of the **E** vector position angles, χ, was set by observations of 3C 286, which was assumed to have $\chi=33°$ at both frequencies. The polarization position angle data were corrected for the effects of ionospheric Faraday rotation using measurements of electron content from the World Data Centre. The systematic errors in χ, estimated from the scatter in the measurements for 3C 286, are <1° at 4.9 GHz and <3° at 1.4 GHz.

This paper presents polarimetry of 3C 272.1 at 3.86 arcsec (290 pc) resolution. The radio images were constructed, self-calibrated and deconvolved using AIPS image processing packages at NRAO and at Jodrell Bank. The shortest (projected) baselines in the data are 106 m at 1.4 GHz and 32 m at 4.9 GHz, corresponding to fringe separations of 6.8 arcmin at 1.4 GHz and 6.4 arcmin at 4.9 GHz. As the individual lobes of 3C 272.1 have diameters <2 arcmin, the only scales to which our images might be insensitive would be those of any 'halo' that might surround both lobes. The integrated flux densities in our final images (estimated by ordinate summation) are

Table 1. VLA observational parameters.

Observing date	1980 November 9	1981 June25	1981 November 17
Frequency	1.413 GHz	1.413 GHz	4.885 GHz
Integration time	2 hr	1 hr	5.5 hr
HA range	±6 hr	±4 hr	±4 hr
Bandwidth	12.5 MHz	25 MHz	50 MHz
Configuration	A	B	C
I image rms/beam	400 μJy	400 μJy	50 μJy
Q, *U* image rms/beam	175 μJy	170 μJy	40 μJy
Primary HPBW	31 arcmin	31 arcmin	9.2 arcmin

6.35 Jy at 1.4 GHz and 2.79 Jy at 4.9 GHz. The integrated flux densities from single-dish observations are 6.33±0.23 Jy at 1.4 GHz (Bridle *et al.* 1972, adjusted to the Baars *et al.* scale) and 2.88±0.09 Jy at 4.9 GHz (interpolated from Laing & Peacock 1980). We therefore believe that <0.1 Jy is likely to be in a large-scale halo that would be 'missing' from our images at either frequency. Even if 0.1 Jy were contained in a symmetrical Gaussian region with a FWHM of 2.8 arcmin (the angular scale on which our sensitivity falls to one-half), the surface brightness of such 'missing' emission would be only 26 μJy per CLEAN beam area at our resolution. Its contribution would therefore be well below the rms noise in our 1.4-GHz images, and below the noise in our 4.9-GHz images. Our VLA polarimetry is therefore unlikely to be biased significantly by the effects of any emission from 3C 272.1 that has been inadequately sampled.

We have also used observations made at 2.695 GHz with the Cambridge 5-km telescope, communicated to us by J. M. Riley. These data, incorporating observations made on 64 baselines, were obtained and calibrated as described by Laing (1981). They were CLEANed and restored with an elliptical Gaussian beam of FWHM 3.86 arcsec in RA and 16.25 arcsec in Dec. Images at this resolution were also made from the VLA data at 1.4 and 4.9 GHz, for comparison with the 2.7-GHz results.

3 Total and polarized emission

3.1 TOTAL INTENSITY

Fig. 1 shows contours of the total intensity (Stokes *I*) at 4.9 GHz to illustrate the main structural features of the radio source at 3.86-arcsec resolution. An unresolved core in the nucleus of the galaxy is linked by two resolved jets to a pair of broad lobes. The jets leave the nucleus in position

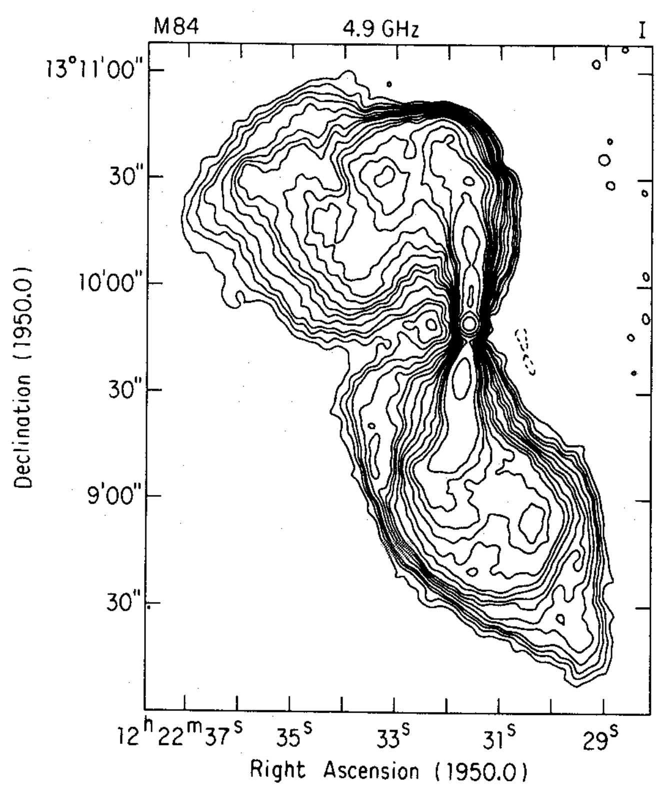

Figure 1. Total intensity distribution at 4.9 GHz, from VLA *C* configuration data at 3.86-arcsec resolution. Contours are drawn at 0.2, 0.4, 0.6, 0.8, 1.2, 1.6, 2.0, 2.4, 3.2, 4.0, 4.8, 6.4, 8.0, 9.6, 12.8, 25.6, 51.2 and 102.4 mJy per CLEAN beam area.

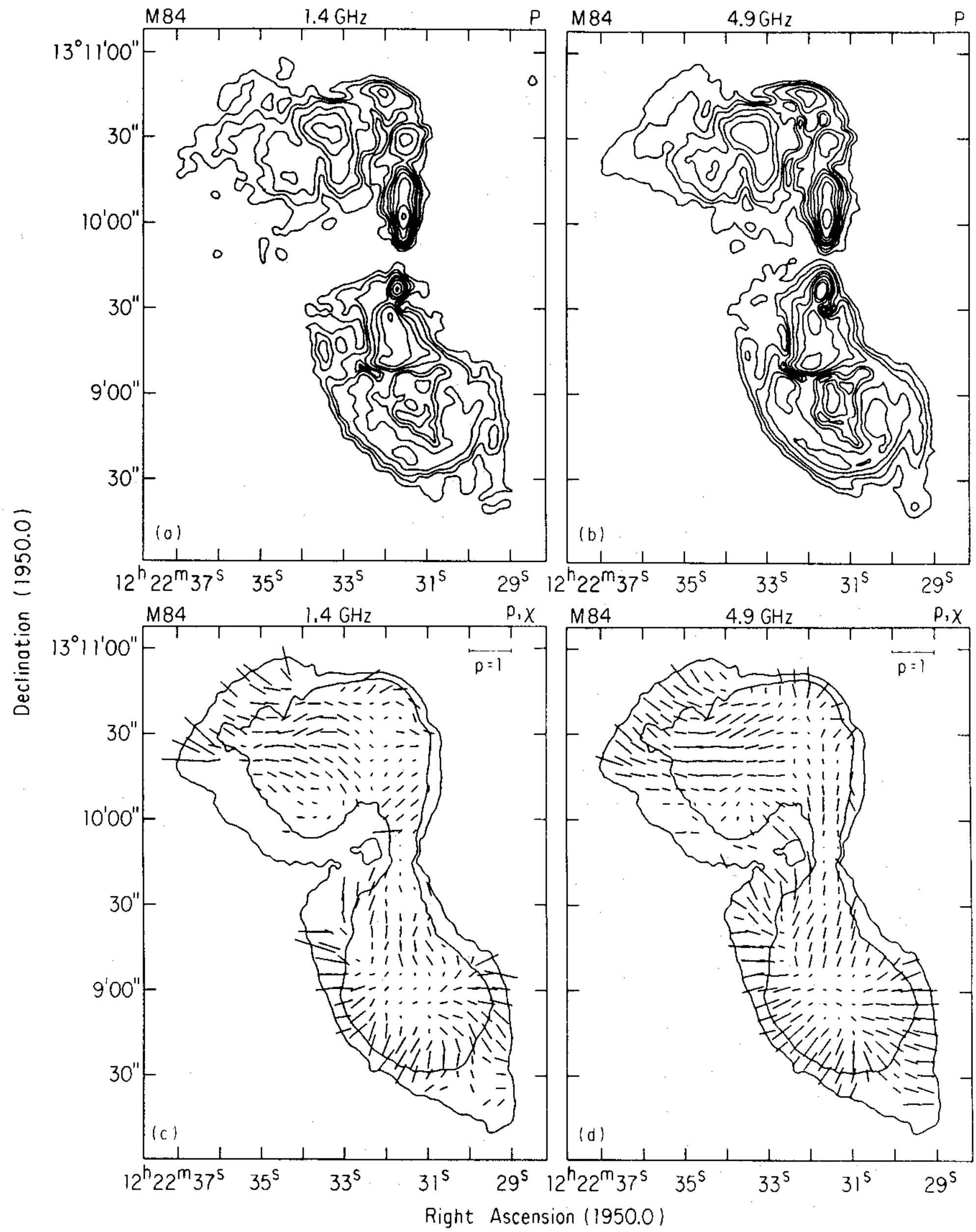

Figure 2. Distributions of polarized intensity (upper panels) and **E** vector position angles (lower panels) at 3.86-arcsec resolution at 1.4 GHz (left panels) and 4.9 GHz (right panels). (a) Contours are drawn at 0.72, 1.44, 2.2, 3.6, 5.0, 7.2, 10.8, 14.4 and 22 mJy per CLEAN beam area. (b) Contours are drawn at 0.3, 0.6, 0.9, 1.5, 2.1, 3, 4.5, 6 and 9 mJy per CLEAN beam area. These levels are chosen so that if the polarized intensity had the same spectral index as the total intensity (i.e. if there was no depolarization) there would be the same number of contours at each location in both plots. The vectors in the lower panels have lengths proportional to the degree of polarization p at each frequency (the length of the vector corresponding to $p=1$ is shown at the upper right of each panel). No vectors are shown where the polarized signal-to-noise ratio is $<4:1$. The vectors are shown slightly undersampled, at 5 arcsec intervals, for clarity.

angles of $\sim -5°$ and $+170°$ and are fairly straight for $\sim$40 arcsec, at which distance from the core they both deflect to the east before merging with the broader lobe emission. The jets are surrounded by a broad, conical 'cocoon' of faint radio emission whose outer parts also blend with the lobes at the resolution of Fig. 1.

The south lobe contains an 'inner lobe' that is separated from more diffuse outer structure by steep brightness gradients. The steepest gradients occur at the north-west corner of the source, where the north jet deflects eastward and blends with more diffuse emission, and around the south 'inner lobe', especially on its south-east and north-west sides. The south-east boundaries of the diffuse emission around both lobes are also marked by enhanced brightness gradients.

A 4.9-GHz image of 3C 272.1 at 1.2-arcsec resolution (Bridle & Perley 1984) shows that the north jet is much brighter than the south jet for the first ~10 arcsec from the core, i.e. that the brightness symmetry displayed by the jets on the scale of Fig. 1 develops ~750 pc from the nucleus.

3.2 POLARIZED EMISSION

Fig. 2(a) and (b) display contours of the linearly polarized intensity ($P=\sqrt{Q^2+U^2}$) at 1.4 and 4.9 GHz. Fig. 2(c) and (d) show vectors whose lengths are proportional to the degree of polarization $p=P/I$ and whose position angles χ are those of the observed **E** vectors. Most of our conclusions about the polarization properties of the source are limited by the noise in the 1.4-GHz data shown in Fig. 2(a) and (c). The distributions of degree of polarization p and of depolarization $D^{1.4}_{4.9}=p_{1.4}/p_{4.9}$ referred to here and in Section 6 have been corrected for the bias in the Ricean distribution of P (e.g. Wardle & Kronberg 1974) using the values listed in Table 1 for the standard deviations of the Gaussian distributions of Q and U.

The lobes and the jets are highly linearly polarized at 3.86-arcsec resolution at both frequencies. The degree of polarization $p_{4.9}$ at 4.9 GHz is between 0.15 and 0.3 over much of the jets, and

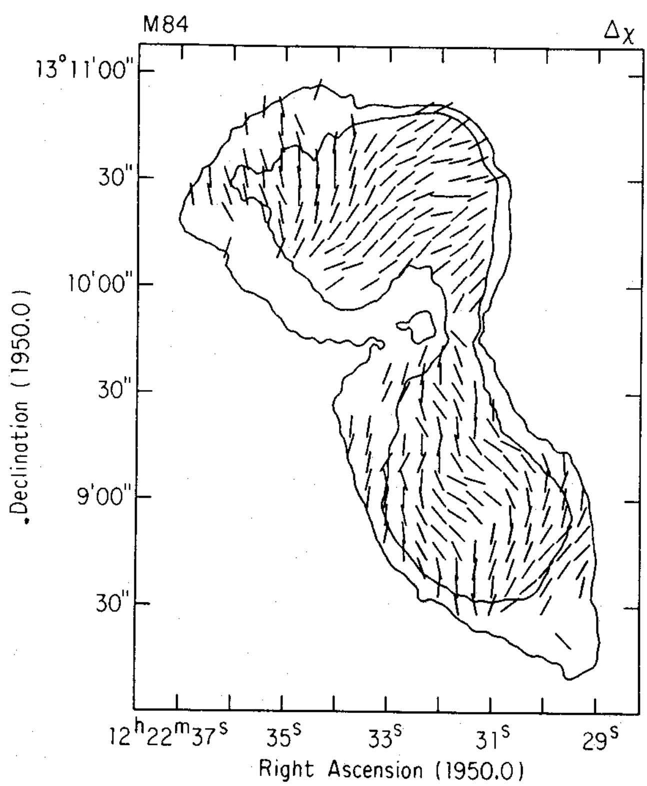

Figure 3. Distribution of position angle differences $\Delta\chi$ between the electric vectors at 1.4 and 4.9 GHz with 3.86-arcsec resolution. The vectors are of unit length, and are drawn at angles representing $\Delta\chi$ positive counter-clockwise from zero (vertical). The contours are the 0.4 and 2.4 mJy per CLEAN beam area levels from Fig. 1. No vectors are shown where the polarized signal-to-noise is <5:1 at either frequency. As in Fig. 2, the vectors are shown slightly undersampled, at 5 arcsec intervals, for clarity.

is between 0.3 and 0.45 over much of both lobes. The highest values of $p_{4.9}$ are between 0.45 and 0.55, and occur on the steep brightness gradients that separate the south 'inner lobe' from the more diffuse emission around it – see Fig. 2(d). The main regions of low polarization at this resolution are east of the north jet, south and east of the south jet, and near the centre of the south lobe; in these regions $p_{4.9} \leqslant 0.05$ at some points. The apparently low degrees of polarization near the edges of the jets may partly result from beam smearing of the **E** vector pattern, as there are significant changes in the orientations of neighbouring 4.9-GHz **E** vectors in these regions at this resolution. Fig. 2(a) and (b) show that the distributions of the polarized intensity at 1.4 and 4.9 GHz are generally similar, except in a few localized regions which we discuss further in Section 6.

4 Rotation

4.1 E VECTOR ROTATION BETWEEN 1.4 AND 4.9 GHz

The generally high degree of linear polarization at both frequencies allows us to map the rotation $\Delta\chi = \chi_{1.4} - \chi_{4.9}$ of the position angle χ of the observed **E** vectors between 1.4 and 4.9 GHz over most of the source. Fig. 3 shows this position angle rotation $\Delta\chi$ in a vector display superimposed on selected intensity contours from Fig. 1. The values of $\Delta\chi$ are, of course, ambiguous to $\pm 180n°$. Fig. 3 displays rotation data without resolving this ambiguity, i.e. without imposing any assumptions about the value of n.

Fig. 3 reveals a coherent two-dimensional pattern of the rotation $\Delta\chi$ over the radio source. $\Delta\chi$ differs significantly from zero over much of both lobes and the jet, and adjacent measures of $\Delta\chi$ are strongly correlated. Whatever produces the rotation clearly has structure on a scale $\geqslant 20$ arcsec ($\geqslant 1.5$ kpc). The high degree of ordering of the rotation suggests that n is constant over most of the source, so we initially take n to be zero. (We justify this assumption in Section 4.3).

4.2 EQUIVALENT ROTATION MEASURE

We assume that the rotation is caused by the Faraday effect (Faraday 1846) in a magnetoionic medium. Figs 4 and 5 therefore present two further visualizations of the rotation pattern, obtained by converting it to an equivalent rotation measure $RM_{4.9}^{1.4}$ using the relation

$$RM_{4.9}^{1.4} = \frac{\Delta\chi}{\lambda_{1.4}^2 - \lambda_{4.9}^2}$$

i.e. by transforming it into the smallest range of $RM_{4.9}^{1.4}$ that is consistent with the $\Delta\chi$ data (see Section 4.3). The equivalent rotation measures range from -35 rad m^{-2} to $+25$ rad m^{-2}.

Fig. 4 shows a grey-scale representation of the distribution of $RM_{4.9}^{1.4}$ superimposed on selected contours from the total intensity map shown in Fig. 1. Values of the RM are not represented in the grey-scale display in Fig. 4 wherever the polarized signal-to-noise is <6:1 at either frequency. This criterion eliminates regions where the RM values are less certain because of limited sensitivity or because $\chi_{1.4}$ or $\chi_{4.9}$ varies significantly across our 3.86-arcsec beam.

The most striking feature of Fig. 4 is that the deviations from $RM_{4.9}^{1.4} = 0$ oscillate over the source, the steepest gradients in $RM_{4.9}^{1.4}$ being along position angle $50 \pm 2°$. The largest positive rotations are in a band across the centre of the north lobe, passing through the region where the north jet deflects eastwards. The largest positive rotations are in a band crossing the centre of the south lobe.

The extrema of the rotation measure distribution are correlated with the steepest brightness

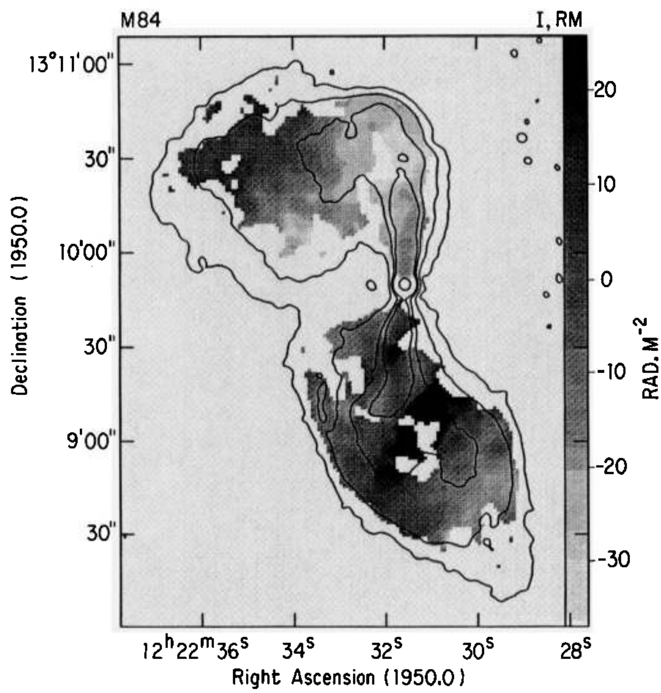

Figure 4. Grey-scale representation of the distribution of equivalent Faraday rotation measure $RM^{1.4}_{4.9}$ across the source, superimposed on the 0.2, 1.6, 6.4, 12.8 and 102.4 mJy per CLEAN beam contours from the total-intensity map shown in Fig. 1. Areas of the grey-scale display in which the polarized signal-to-noise ratio is <6:1 at either frequency have been left blank.

[*facing page* 562]

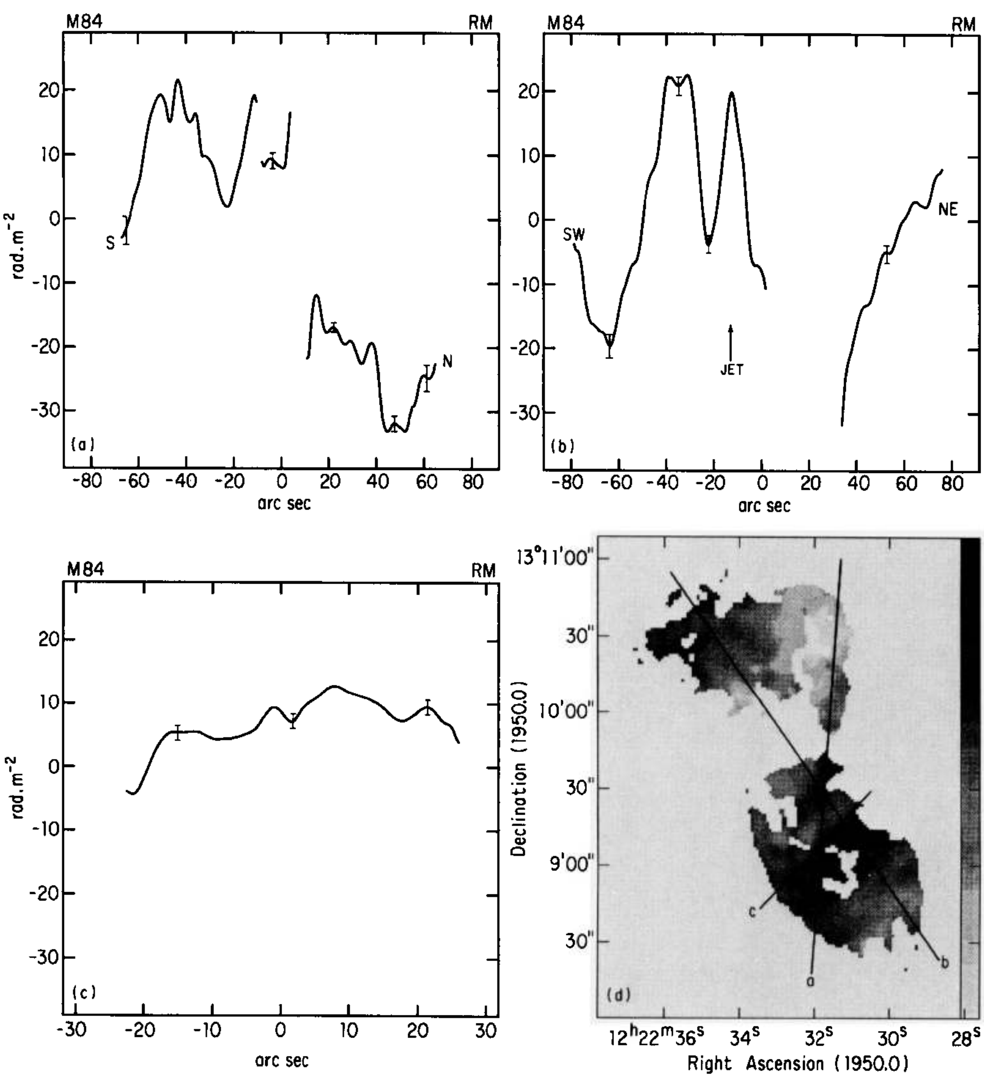

Figure 5. Cuts through the equivalent Faraday rotation measure distribution along the tracks shown as solid lines in panel (d). Note that (a) and (b) have the same angular scale, and that the *RM* data are again excised wherever the polarized signal-to-noise ratio is <6:1 at either frequency. Representative 1σ errors are also shown.

gradients at the edges of the source – in both lobes, the loci of the highest positive and negative rotations cross the edges of the source near their steepest brightness gradients. There is also a band of large negative rotations in the south lobe on the south-west rim of the 'inner lobe', i.e. on the steep brightness gradient that separates this inner lobe from fainter emission to the south-west. As the position angles χ depend only on the *ratios* of the Stokes parameters Q and U, instrumental effects cannot produce such a correlation between RM and brightness gradient.

The steepest gradients in $RM_{4.9}^{1.4}$ are ≈ 4 rad m^{-2} arcsec^{-1} and occur along the edges of the south jet and across the centre of the south lobe. There are also gradients of ≈ 3 rad m^{-2} arcsec^{-1} near the edges of the north jet and at the south-east edge of the north lobe.

Fig. 5(a), (b) and (c) display profiles through the RM pattern, along each of the three tracks shown as solid lines in Fig. 5(d). The profile taken along the jets, shown in Fig. 5(a), exhibits an abrupt change of the sign of the rotation measure across the nucleus of M84, from +15 to −15 rad m^{-2} going from south to north. The principal variations of RM are smooth and well resolved, as evidenced by Fig. 5(b). Maps of $RM_{4.9}^{1.4}$ at 1.75-arcsec resolution confirm that there is no significant smaller scale structure in the rotation measure (they are not shown here as they have generally lower signal-to-noise ratio and add no further detail). There is, however, a small region with an anomalous RM of about +15 to +20 rad m^{-2} relative to the larger scale variations, about halfway along the south jet (around $\alpha \approx 12^h 22^m 31^s.8$, $\delta \approx +13° 09' 25''$), as can be seen from Figs 4 and 5(b). In the parts of the south lobe that are well removed from the jets, there is little variation in $RM_{4.9}^{1.4}$ at right angles to the steepest RM gradient, i.e. along position angle ~140° – as in Fig. 5(c).

4.3 TESTING THE λ^2 LAW

Observations of the **E** vector position angles at a third radio frequency are needed to decide whether the magnetoionic medium is in front of, or within, the radio source, and to establish whether there are ambiguities of $\pm 180n°$ in $\Delta\chi$. The only suitable intermediate-frequency data available to us are at 2.7 GHz from the Cambridge 5-km telescope at a resolution of 3.86 arcsec in RA by 16.25 arcsec in Dec. The beam of this instrument in declination is unfortunately similar to the scale of the fluctuations in $RM_{4.9}^{1.4}$ over much of the source. These 2.7-GHz data do, however, permit a rough test of the χ versus λ^2 law wherever RM varies only slowly with declination, and also allow us to check for possible rotational ambiguities, using the following procedure.

We first predicted the orientations of the 2.7-GHz **E** vectors at 3.86-arcsec resolution from those at 1.4 and 4.9 GHz, assuming that $\Delta\chi \propto \lambda^2$ and $n=0$. We made this prediction using the observed values of $p_{4.9}$ to determine the values of Q/I and U/I at 2.7 GHz at this resolution. This only approximates the correct procedure, which would be to interpolate the 2.7-GHz I distribution at 3.86-arcsec resolution and hence to estimate Q and U directly; the approximation is a good one for our purpose, because the spectral index of the polarized emission does not vary significantly over the source. The resulting Q/I and U/I distributions were then convolved to the 16.25-arcsec Dec resolution of the Cambridge 5-km telescope and the smoothed distribution of χ at 2.7 GHz was predicted from the smoothed Q/I and U/I distributions.

Fig. 6 shows vectors whose position angles are the *differences* $\Delta\chi$ between the predicted values of $\chi_{2.7}$ and those observed with the Cambridge 5-km telescope. The vector lengths in Fig. 6 are proportional to the observed distribution of $P_{2.7}$, to show the relative signal-to-noise ratio at each point. If our assumption of minimal RM is correct, these vectors should all be vertical, apart from the effects of noise.

The mean position angle difference $\Delta\chi$ shown in Fig. 6 is 2°.1, with a variance of 6°.7. The mean error in the observed 2.7-GHz position angles used in this comparison was 4°.0, so the variance of the position angle differences in Fig. 6 is evidently dominated by the noise in the data, rather than

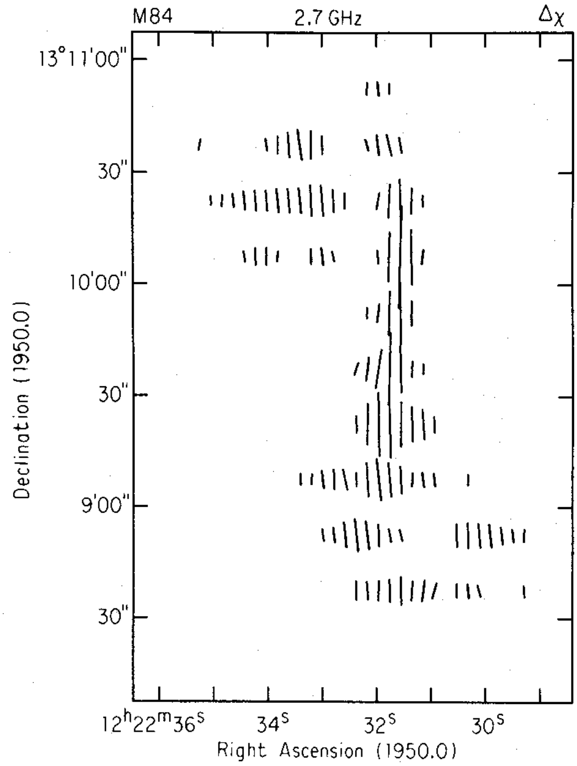

Figure 6. Distribution of the difference $\Delta\chi$ between observed and predicted **E** vector position angles at 3.86 by 16.25 arcsec resolution at 2.7 GHz, assuming that the *RM* has the minimum values consistent with the data at 4.9 and 1.4 GHz. The lengths of the vectors are proportional to the polarized intensities at 2.7 GHz. Vectors are drawn only where the signal-to-noise ratio in the observed distribution is >4:1.

by discrepancies from the λ^2 law of rotation. The only significant differences between the predicted and observed vector orientations are also in regions of low polarized intensity.

These comparisons show that there is no $180n°$ ambiguity in $\Delta\chi$, that $n=0$, and that $\Delta\chi$ is at least approximately proportional to λ^2 over most of the source. There is, however, a region at the south-eastern edge of the north lobe (from $\alpha \approx 12^h 22^m 34^s.2$, $\delta \approx +13° 10' 00''$ to $\alpha \approx 12^h 22^m 35^s.5$, $\delta \approx +13° 10' 25''$) containing some locally unusual rotation measure gradients, and possible departures from the $\Delta\chi \propto \lambda^2$ law. Part of this region also depolarizes significantly at 1.4 GHz (see Section 6).

At those points in the source where the higher-resolution maps show little variation in $RM_{4.9}^{1.4}$ across the Cambridge 2.7-GHz beam, we have directly tested the hypothesis that $\Delta\chi \propto \lambda^2$. Fig. 7 shows a few representative fits of this law to the data at such points. This analysis also shows no evidence for any deviation from the λ^2 law over a maximum $\Delta\chi$ of 80°.

5 The magnetic field in the source

We have converted the values of $\chi_{4.9}$ to infinite frequency using the $\Delta\chi \propto \lambda^2$ law appropriate for a foreground Faraday screen as justified above. Fig. 8 shows the implied distribution of 'intrinsic' apparent magnetic field across the radio source at 3.86-arcsec resolution. The field lines wrap around the edge of the 'inner' lobe in the south half of the source. In the jet-dominated regions, the field lines are generally perpendicular to the ridge line of the jet, but they stretch around the outside of the bend of the north jet (at the north-west corner of the source).

Where there are steep brightness gradients in the lobes and the magnetic field pattern has also

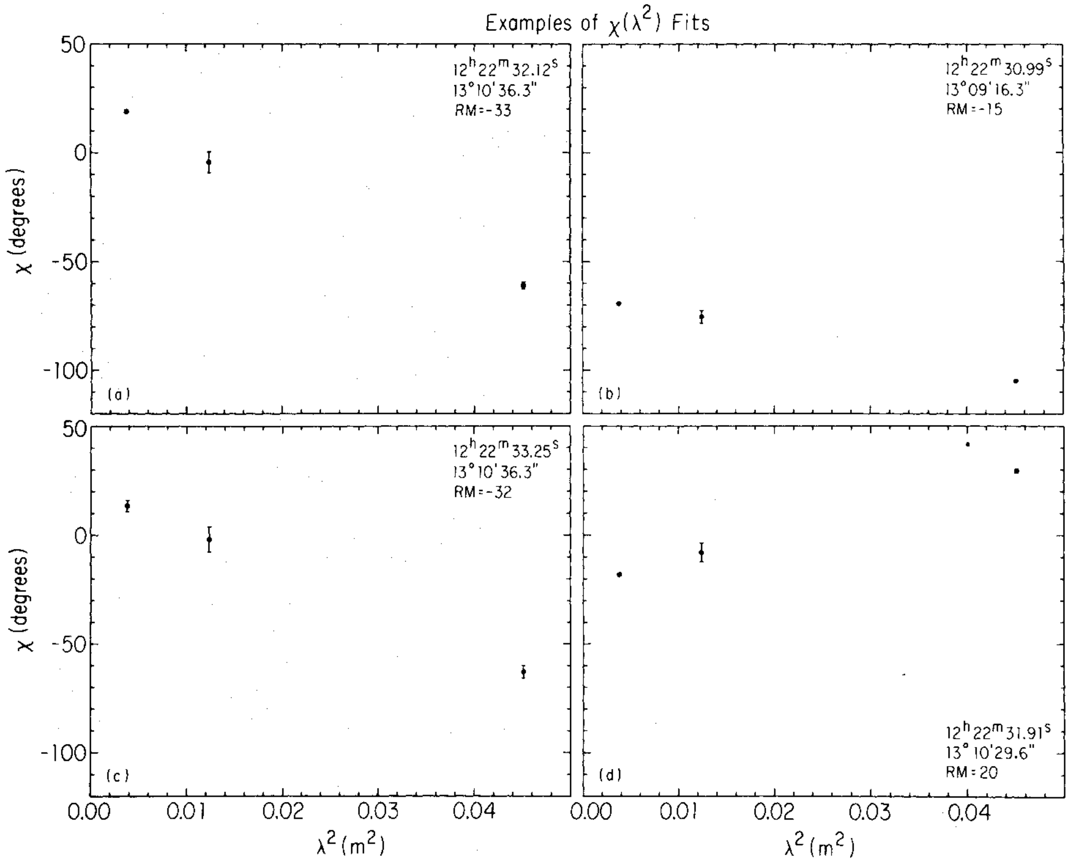

Figure 7. Plots of χ versus λ^2 for the positions indicated in the corner of each panel.

been well resolved, the field is generally perpendicular to the brightness gradient. The only significant exception to this occurs in the region between $\alpha \approx 12^h 22^m 34\overset{s}{.}2$, $\delta \approx +13° 10' 00''$ and $\alpha \approx 12^h 22^m 35\overset{s}{.}5$, $\delta \approx +13° 10' 25''$ along the south-eastern edge of the north lobe. This region has unusual rotation measure gradients and possible local departures from the $\Delta\chi \propto \lambda^2$ law (Section 4.3).

These features are similar to magnetic field distributions commonly seen in radio lobes and two-sided radio jets in other active galaxies (e.g. Bridle & Perley 1984; Burch 1979; Högbom 1979; van Breugel & Fomalont 1984). This reinforces our conclusion that the observed **E** vector rotation is caused by the Faraday effect with $\Delta\chi \propto \lambda^2$ over most of the source.

6 The magnetoionic medium

The above observations do not determine where the Faraday screen is located along the line-of-sight between us and 3C 272.1. Several arguments suggest, however, that the screen is mainly in a foreground medium close to M84 itself, rather than in our own Galaxy.

The source is at galactic coordinates $l = 278\overset{\circ}{.}2$, $b = 74\overset{\circ}{.}5$, a region of sky where the *integrated* rotation measures of other extragalactic sources are generally small. Simard-Normandin, Kronberg & Button (1981) list the values of *RM* for 11 extragalactic sources within 10° of 3C 272.1. The *RM* of M87 (3C 274) is wildly discrepant from all the others, so we presume it to be intrinsic to M87 and neglect it in what follows. The unweighted mean *RM* for the other 10 sources is $-2.4 \pm 3.9\,\mathrm{rad\,m^{-2}}$, corresponding to a rotation $\Delta\chi$ of $-6 \pm 9°$ between 4.9 and 1.4 GHz. We therefore expect the mean foreground (galactic) contribution to the *RM* to be near zero. The *RM*s

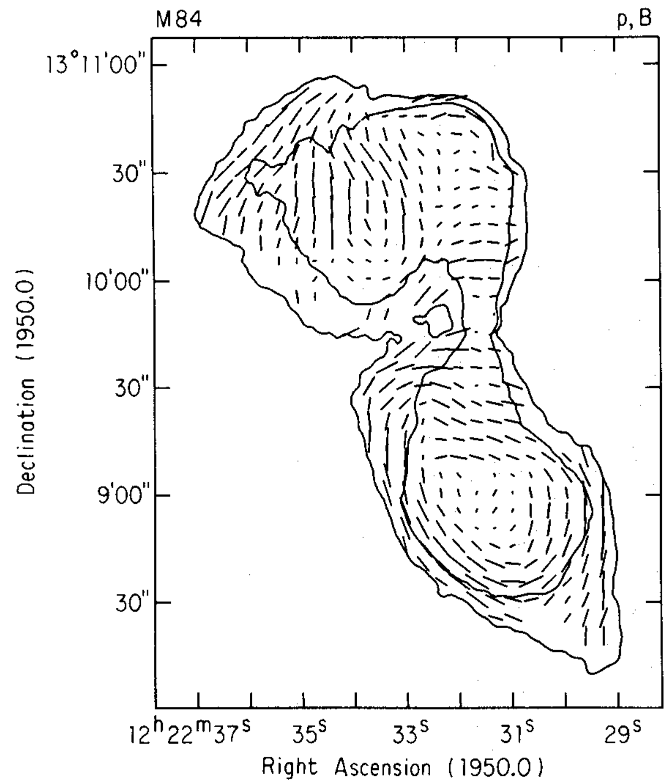

Figure 8. The apparent (i.e. weighted by synchrotron emissivity and vector averaged) magnetic field distribution $\mathbf{B}_a$ over the source at 3.86-arcsec resolution, after correction for the Faraday rotation measure distribution shown in Fig. 4 assuming that $\Delta\chi \propto \lambda^2$. The vector lengths are proportional to the degree of linear polarization $p_{4.9}$ at 4.9 GHz, as this measures the degree of orderliness of the magnetic field. The vector orientations show the directions of $\mathbf{B}_a$.

of the other 10 sources also provide no evidence for any systematic structure of the foreground *RM* in this area of sky over scales of order 1–5 degrees.

These integrated *RM* data do not give evidence for or against the existence of fluctuations in the galactic foreground *RM* in this direction on scales smaller than those of the single-dish beams that were used to determine the *RM*s. Recent interferometric studies of *RM* distributions across extragalactic radio sources at a variety of galactic latitudes (Leahy 1985; Simonetti & Cordes 1986) do, however, show that excursions of $\pm 25\,\mathrm{rad\,m^{-2}}$ in $RM^{1.4}_{4.9}$ over a scale of only a few arcmin, as in M84, would be unusual even in the regions at low galactic latitudes that show large-scale *RM* 'anomalies'. These interferometric studies show that, at high galactic latitudes, foreground *RM* fluctuations on arcmin scales are rarely more than a few $\mathrm{rad\,m^{-2}}$. The contribution of the galactic foreground to the *RM* distribution over M84 should therefore be near zero in the mean, with fluctuations comparable to, or less than, the 'noise' in Fig. 5.

Note also that the *RM* cut shown in Fig. 5(a) shows an abrupt change in the sign of the *RM* across the nucleus of M84. This is also evidence against a galactic foreground origin for the screen, as the coincidence between this abrupt change and the centre of M84 would be 'accidental' if the screen is unrelated to M84 itself.

The following observations, while not conclusive, suggest that the Faraday-rotating medium is within the inner few kpc of M84 but in front of the radio source, rather than being significantly mixed with the radio-emitting plasma.

(i) $\Delta\chi \propto \lambda^2$ over a rotation of $\Delta\chi \approx 80°$, which is consistent with the medium being in front of the radio source, rather than being mixed with it (Burn 1966; Laing 1985).

(ii) In a mixed geometry, the radio polarization and Faraday rotation are produced by

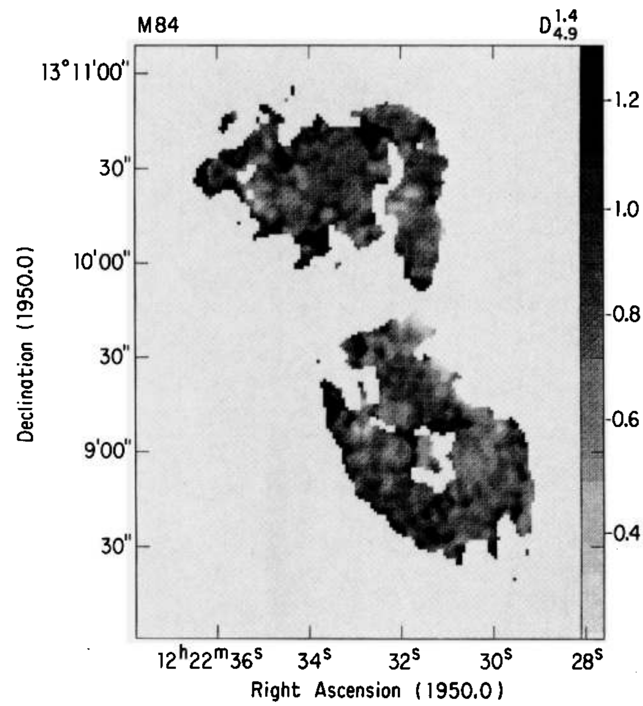

Figure 9. Grey-scale representation of the distribution of the depolarization $D^{1.4}_{4.9}=p_{1.4}/p_{4.9}$ over the source, at 3.86-arcsec resolution.

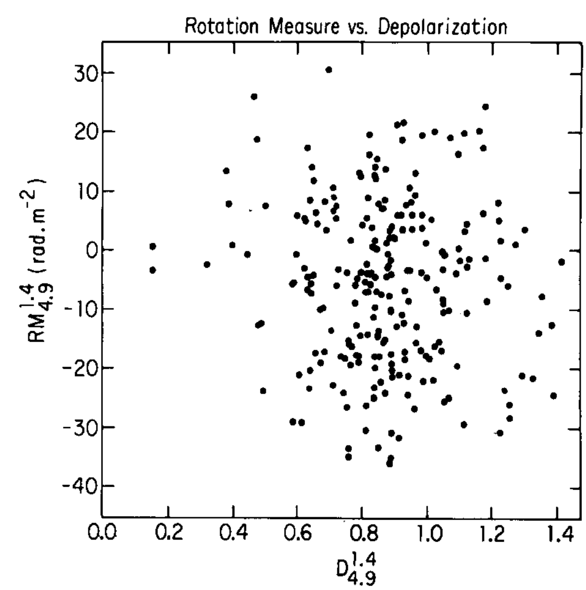

Figure 10. Plot of the rotation measure $RM^{1.4}_{4.9}$ against the depolarization $D^{1.4}_{4.9}=p_{1.4}/p_{4.9}$ for locations at 5 arcsec intervals across the radio source, showing the lack of detailed correlation between these two quantities. The largest uncertainties in individual data points are $\pm 4\ \mathrm{rad\ m^{-2}}$ in RM and ± 0.3 in D; typical uncertainties are 2–3 times smaller.

[*facing page* 566]

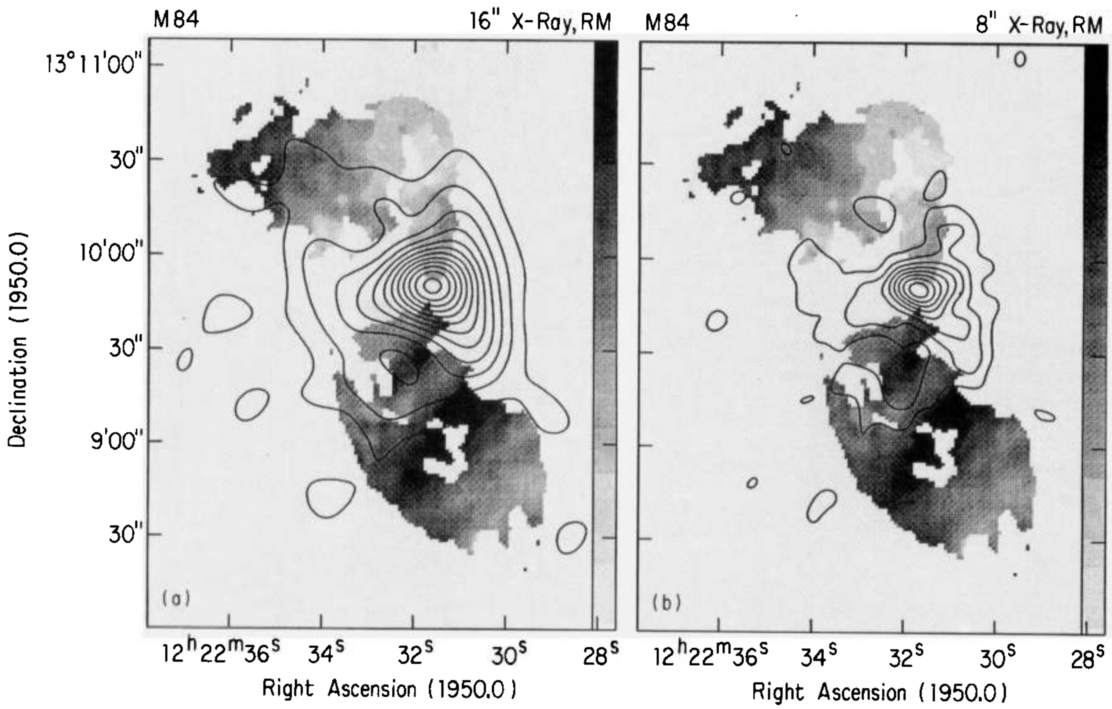

Figure 11. Contours of the X-ray intensity (linear contour levels) measured by the *Einstein* HRI superimposed on the grey-scale representation of the Faraday rotation measure from Fig. 4. The X-ray data in panel (a) have been smoothed with a Gaussian of FWHM 16 arcsec; those in panel (b) with a Gaussian of FWHM 8 arcsec.

(orthogonal components of) the same magnetic field and should therefore be corrrelated to some extent. This is not observed to be the case. The lack of correlation is consistent with most of the rotation occurring in front of, but not inside, the radio source.

(iii) The observed values of the depolarization $D_{4.9}^{1.4}=p_{1.4}/p_{4.9}$ (displayed as a grey-scale image in Fig. 9) show no detailed correlation with $RM_{4.9}^{1.4}$ (compare Figs 4 and 9), although there are some small regions of significant depolarization. If the thermal matter producing as much as 35 rad m^{-2} of rotation were uniformly mixed with the synchrotron material, then simple slab models would predict a correlation between $D_{4.9}^{1.4}$ and $RM_{4.9}^{1.4}$, with $D_{4.9}^{1.4}$ decreasing to near zero in the regions of most deviant *RM*. Fig. 9 shows no evidence of a large-scale banded pattern in $D_{4.9}^{1.4}$ like that in *RM* (Fig. 4), however. Furthermore, Fig. 10, which plots the values of $D_{4.9}^{1.4}$ against those of $RM_{4.9}^{1.4}$ at 5 arcsec intervals over the whole source, also shows no sign of a global correlation between depolarization and rotation over 3C 272.1

(iv) The small scale of the observed *RM* fluctuations, and the abrupt change in sign of the *RM* across the nucleus of M84, make it unlikely that the fluctuations are imposed by a medium that is distributed along the line-of-sight to M84 through the atmosphere of the Virgo cluster as a whole.

We therefore conclude that most of the observed rotation arises in a component of the interstellar medium of M84 that lies in front of the radio source.

There is ample independent evidence for a significant interstellar medium in M84, namely the dust lane (Wade 1960; Hansen *et al.* 1985), the extended optical line emission (Hansen *et al.* 1985) and the extended soft X-ray source (Forman *et al.* 1984, 1985).

Hansen *et al.* estimate that the brightest optical line-emitting regions in M84 contain ionized material at a density of $n_e \sim 10^3$ cm^{-3} and a temperature $T \sim 10^4$ K, with a volume filling factor of $\sim 10^{-8}$. We note, however, that this gas is most unlikely to cause a coherent large-scale pattern of Faraday rotation, such as that seen here, because the scale size that Hansen *et al.* deduce for the line-emitting clouds ($\leq 10^{-2}$ arcsec) is much smaller than our radio beam. This gas is much more likely to cause beam depolarization than to produce a large-scale pattern in the rotation measure. Similar physical conditions occur in the Crab Nebula (Swinbank 1980; Wilson, Samarasinha & Hogg 1985), where emission line filaments evidently depolarize background radio emission. This process also appears to be significant in radio galaxies such as 3C 305 (Heckman *et al.* 1982) and 3C 277.3 (van Breugel *et al.* 1985), where the strengths of optical line emission and the degrees of linear polarization at centimetre wavelengths are anticorrelated.

The only region of 3C 272.1 where an emission line feature imaged by Hansen *et al.* overlaps the radio source is at the north end of the south jet, about 8 arcsec south of the core. This is indeed the most depolarized part of the source, having $D_{4.9}^{1.4} \sim 0.3$, so it is possible that this depolarization feature is related to the presence of the emission line gas. The reality of the line feature in this region of the Hansen *et al.* data is questionable, however.

$D_{4.9}^{1.4}$ falls to ~ 0.45 for a few arcsec around $\alpha \approx 12^h 22^m 35^s.2$, $\delta \approx +13° 10' 20''$, and to ~ 0.5 at a few places near the eastern edges of both jets, and on the western edge of the south lobe. The observation that the distribution of $D_{4.9}^{1.4}$ contains a few such concentrated features suggests that they are produced by a medium with a smaller clumping scale than that responsible for the large-scale variation of *RM*. It will be of interest to search these areas of M48 for optical line emission. In contrast, the extended X-ray emitting gas appears to have the right angular scale to produce the observed rotation pattern if it is threaded by magnetic field of only modest strength. Fig. 11 superimposes the *Einstein* HRI X-ray images smoothed by Gaussians of (a) 16 arcsec FWHM and (b) 8 arcsec FWHM on the grey-scale image of the *RM* variations. Fig. 11 shows that, although the Faraday rotation cannot be produced by the gas which contributes the *brightest* features of the observed X-ray distribution (panel b), it may be produced by gas that contributes to the weaker, more diffuse, X-ray emission, as this covers much of 3C 272.1 (panel a).

A slab of ionized gas with electron density n_e cm^{-3}, field strength B μG and thickness L kpc along the line-of-sight produces a Faraday rotation $RM=810 n_e BL$ rad m^{-2}. To produce $RM \approx 25$ rad m^{-2} requires $\int n_e B dl \approx 0.03\,\mu$G cm^{-3} kpc for the foreground magnetoionic medium in M84. To estimate the magnetic field strength that is needed in the X-ray emitting gas to meet this condition, we have integrated $\int n_e dl$ through the front half of a King model atmosphere with a core radius of 2 kpc, a 0.5 to 3 keV luminosity of 3×10^{40} erg s^{-1} and a temperature of 1.2×10^{7} K (equivalent to 1 keV) – the mean parameters of M84's extended X-ray emission as estimated by Forman *et al.* (1985). This model predicts $\int n_e dl = 0.2$ cm^{-3} kpc, of which 0.11 cm^{-3} kpc occurs in the region >1 kpc from the centre of M84. We infer that an average line-of-sight field strength ≈ 0.15–$0.3\,\mu$G would be sufficient to produce the observed RM if the magnetoionic medium is distributed as in this King model. A higher line-of-sight field, $\approx 1.5\,\mu$G, would be required if the medium is in a uniform slab whose thickness is similar to the ~2 kpc scale of the observed RM fluctuations. In either case, the field strength in the Faraday-rotating medium would be well below the equipartition magnetic field strength in the radio lobes, which is $\approx 20\,\mu$G assuming that the radio spectrum is a power law between 10 MHz and 100 GHz, that equal energies reside in relativistic electrons and in 'ions', and that the lobes are fully filled with relativistic particles and field. The magnetic energy stored in the polarization-rotating medium need only be $\leqslant 1$ per cent of the thermal energy if the rotation is indeed produced by gas at the temperatures characteristic of the X-ray, rather than the optical line, emission.

The banded pattern of the RM variations also demands interpretation. Unless our three-frequency picture of the rotation in terms of minimal variations around the mean is incorrect, the mean line-of-sight component of the magnetic field in the Faraday-rotating screen must be oppositely directed in the regions producing the largest RM excursions in the north and south radio lobes. This implies a large-scale organization of the field, such as might be produced by 'combing' of the field by the outflow associated with the radio source. The Faraday rotation data do not, however, determine the three-dimensional structure of the field uniquely, so we will not discuss a detailed model.

As the largest values of RM occur in bands that cross the lobes on their steepest brightness gradients, one might wonder if n_e and/or B in these regions has been increased by an interaction with the radio source. The *brightest* X-ray emission appears to be anticorrelated with the radio emission, as shown by Fig. 11(b). The X-ray peak around the nucleus of M84 is elongated at right angles to the radio jets, suggesting that this gas may have participated in the collimation of the jets. There is also an elongated region of enhanced X-ray emission ≈ 1 arcmin in extent to the west of the jets (this feature points roughly toward the regions of highest and lowest RM in the source) and another extending across the gap between the two radio lobes in the eastern part of the source. These relationships all suggest that the hot gas and the radio source may indeed have interacted. The minimum pressure in the radio jets at 1 kpc from the core is equivalent to the thermal pressure of gas with $n_e T \approx 10^6$ K cm^{-3}; that in the radio lobes at 3.5 kpc from the core is equivalent to the thermal pressure of gas with $n_e T \approx 10^5$ K cm^{-3}. These conditions are similar to those derived from the X-ray data on these scales if the temperature in the X-ray emitting gas is about 1.2×10^{7} K (i.e. the equivalent of ~1 keV), as estimated by Forman *et al.* (1985). This similarity of the pressures is compatible with the X-ray emitting gas and the radio source having influenced each other. The dynamics of their interaction are not clear from the present data, however. Both the bending of the radio jets and the shape of the X-ray source suggest that they are affected by the motion of M84 through the ambient Virgo cluster atmosphere, further complicating the picture.

An extreme geometry for the field and the gas producing the Faraday rotation would be that of a thin 'magnetoionic sheath' around the radio source in which $n_e BL$ has been amplified by compression of M84's interstellar medium, but it is unlikely that the thickness of any such sheath is <2 kpc, for two reasons. First, our higher-resolution data give no indication of any *RM* structure on scales <2 kpc. Secondly, if the Faraday rotation occurred in a thin sheath of compressed field surrounding the lobes, then both the mean field geometry and the total path length through the sheath should vary between lines-of-sight through the centre and towards the edges of the lobe. We see no evidence for systematic *RM* gradients between the centres and the edges of the lobes that would suggest a sheath scale <2 kpc.

Finally, we note that the loci of constant *RM* away from the jets are in position angle 140±2°, roughly orthogonal to the major axis of the lowest-brightness radio emission in 3C 272.1 (32°, see Fig. 1). This also suggests that the medium causing the Faraday rotation influences the shape of the radio source on scales of several kpc. Furthermore, the steepest *RM* gradients align approximately with the major axis of the large-scale radio structure and with the minor axis of the integrated light of M84 on the scale of the radio source (33° at 1.5 arcmin from the nucleus – King 1978). This coincidence echoes the trend for radio sources to emerge near the stellar minor axes of elliptical galaxies, found by Palimaka *et al.* (1979), Guthrie (1979) and Shaver *et al.* (1982), although the physical basis of this trend is unclear.

7 Conclusions

As noted in Section 1, the results presented here are not the first evidence for a magnetoionic medium in an elliptical radio galaxy. Perley *et al.* (1984) made a detailed multifrequency study of the Faraday rotation measure over the main jet in the giant radio galaxy NGC 6251 (l=116°, b=+37°) and found evidence there for *RM* variations of over 120 rad m^{-2} on a scale of ~15 kpc. In NGC 6251, the highest values of $\Delta\chi$ are considerably larger than those in M84, and $\Delta\chi$ is clearly proportional to λ^2. These results make it certain that most of the rotation in NGC 6251 occurs in a foreground magnetoionic medium with $n_e BL \sim 0.1\,\mu$G cm^{-3} kpc. The *RM* gradients in NGC 6251 are also greatest near the centre of the galaxy; this strengthens the case that the medium is associated with NGC 6251 itself.

O'Dea & Owen (1986) have detected *RM* gradients of ~20–30 rad m^{-2} over distances of ~2–10 kpc respectively along the jets in the head-tail radio galaxy NGC 1265 (l=154°, b=−13°).

Cornwell & Perley (1985) have reported *RM* gradients along the jets in 3C 449 (l=95°, b=−16°), and Leahy, Jägers & Pooley (1986) have detected *RM* gradients of up to ~60 rad m^{-2} over ~3 kpc along the brighter jet in 3C 66B (l=140°, b=−17°). Both of these sources are, however, in a region of sky in which many extragalactic sources have unusually large negative *RM*s. Simard-Normandin & Kronberg (1980) associate this region with a large-scale feature of the galactic magnetic field, and Simonetti & Cordes (1986) show that the *RM* gradients in the region are from three to 10 times greater than those at high galactic latitudes, on all scales that they sampled. The *RM* gradients across 3C 449 and 3C 66B might therefore contain significant components due to foreground material in our own Galaxy.

Finally, Greenfield, Roberts & Burke (1985) have attributed the *RM* difference between the A and B images of the gravitationally lensed quasar 0957+561 (l=158°, b=+48°) to an interstellar medium in the lensing galaxy with $n_e BL \approx 0.1\,\mu$G cm^{-3} kpc.

The shapes of the radio sources in these other galaxies restrict the mapping of their Faraday screens to 'profiles' along (almost) one-dimensional jets, or to single local estimates of Faraday depth. Our data significantly expand this picture by revealing a 'banded' pattern of the rotation measure across M84. To interpret this banded pattern physically, we need to know whether the main *RM* gradients in other galaxies always lie near their major axes, or near the minor axis of their stellar light distributions on the same scale. If there is a single field geometry (outside the radio sources) in all elliptical galaxies, it may be possible to derive it from statistical studies of a randomly-orientated sample. The most critical observations are: (a) accurate multifrequency polarimetry of elliptical radio galaxies, especially those for which there is already X-ray evidence for diffuse extranuclear ionized gas, and (b) a more sensitive study of the distribution of the X-ray emitting gas outside the inner arcmin of M84, to test whether this medium can indeed be identified with the Faraday screen mapped here.

Acknowledgments

We thank Dr W. Forman and Dr F. Seward for sending us a FITS tape with the *Einstein* X-ray image of M84 before the HRI data were published. We also thank the staff of the Cambridge 5-km telescope for obtaining the 2.7-GHz data. We are indebted to M. Classic for valuable contributions to the data reduction at NRAO, and to Dr E. W. Greisen for coding the AIPS task IMVIM that was used to compute Fig. 10. We are grateful to Drs N. Killeen, C. P. O'Dea, J. H. Simonetti and J. V. Wall for valuable advice and criticism, and to an anonymous referee for suggesting several improvements. The hospitality of the Aspen Center for Physics was much appreciated by both authors during the penultimate stage of writing this paper.

References

Baars, J. W. M., Genzel, R., Pauliny-Toth, I. I. K. & Witzel, A., 1977. *Astr. Astrophys. Suppl.*, **61**, 99.
Bridle, A. H. & Perley, R. A., 1984. *Ann. Rev. Astr. Astrophys.*, **22**, 319.
Bridle, A. H., Davis, M. M., Fomalont, E. B. & Lequeux, J., 1972. *Astr. J.*, **77**, 405.
Burch, S. F., 1979. *Mon. Not. R. astr. Soc.*, **186**, 519.
Burn, B. J., 1966. *Mon. Not. R. astr. Soc.*, **133**, 67.
Cornwell, T. J. & Perley, R. A., 1985. In: *Physics of Energy Transport in Extragalactic Radio Sources, Proc. 9th NRAO Workshop*, p. 39, eds Bridle, A. H. & Eilek, J. A., NRAO, Green Bank, West Virginia.
Faraday, M., 1846. *Trans. R. Soc. Lond.*, **136**, 1.
Forman, W. & Jones, C., 1982. *Ann. Rev. Astr. Astrophys.*, **20**, 547.
Forman, W., Jones, C. & Tucker, W., 1984. In: *Clusters and Groups of Galaxies*, p. 297, eds Mardirossian, F., Giuricin, G. & Mezzetti, M., Reidel, Dordrecht, Holland.
Forman, W., Jones, C. & Tucker, W., 1985. *Astrophys. J.*, **293**, 102.
Greenfield, P. E., Roberts, D. H. & Burke, B. F., 1985. *Astrophys. J.*, **293**, 370.
Guthrie, B. N. G., 1979. *Mon. Not. R. astr. Soc.*, **187**, 581.
Hansen, L., Nørgaard-Nielsen, H. U. & Jørgensen, H. E., 1985. *Astr. Astrophys.*, **149**, 442.
Heckman, T. M., Miley, G. K., Balick, B., van Breugel, W. J. M. & Butcher, H. R., 1982. *Astrophys. J.*, **262**, 529.
Högbom, J. A., 1979. *Astr. Astrophys. Suppl.*, **36**, 173.
King, I. R., 1978. *Astrophys. J.*, **222**, 1.
Kotanyi, C. G. & Ekers, R. D., 1979. *Astr. Astrophys.*, **73**, L1.
Laing, R. A., 1981. *Mon. Not. R. astr. Soc.*, **195**, 261.
Laing, R. A., 1985. In: *Physics of Energy Transport in Extragalactic Radio Sources, Proc. 9th NRAO Workshop*, p. 90, eds Bridle, A. H. & Eilek, J. A., NRAO, Green Bank, West Virginia.
Laing, R. A. & Peacock, J. A., 1980. *Mon. Not. R. astr. Soc.*, **190**, 193.
Leahy, J. P., 1985. *PhD thesis*, University of Cambridge.
Leahy, J. P., Jägers, W. J. & Pooley, G. G., 1986. *Astr. Astrophys.*, **156**, 234.
Mould, J., Aaronson, M. & Huchra, J., 1980. *Astrophys. J.*, **238**, 458.
O'Dea, C . P. & Owen, F. N., 1986. *Astrophys. J.*, **301**, 841.
Palimaka, J. J., Bridle, A. H., Fomalont, E. B. & Brandie, G. W., 1979. *Astrophys. J.*, **231**, L7.
Perley, R. A., Bridle, A. H. & Willis, A. G., 1984. *Astrophys. J. Suppl.*, **54**, 292.
Shaver, P., Danziger, I., Ekers, R., Fosbury, R., Goss, W., Malin, D., Moorwood, A. & Wall, J., 1982. In: *Extragalactic Radio Sources, Proc . IAU Symp. No. 97*, p. 55, eds Heeschen, D. S. & Wade, C. M., Reidel, Dordrecht, Holland.
Simard-Normandin, M. & Kronberg, P. P., 1980. *Astrophys. J.*, **242**, 74.
Simard-Normandin, M., Kronberg, P. P. & Button, S., 1981. *Astrophys. J. Suppl.*, **45**, 97.
Simonetti, J. H. & Cordes, J. W., 1986. *Astrophys. J.*, **310**, 160.
Stewart, G. C., Canizares, C. R., Fabian, A. C. & Nulsen, P. E. J., 1984. *Astrophys. J.*, **278**, 536.

Swinbank, E., 1980. *Mon. Not. R. astr. Soc.*, **193,** 451.
van Breugel, W. J. M. & Fomalont, E. B., 1984. *Astrophys. J.*, **282,** L55.
van Breugel, W., Miley, G., Heckman, T., Butcher, H. & Bridle, A., 1985. *Astrophys. J.*, **290,** 496.
Wade, C. M., 1960. *Observatory,* **80,** 235.
Wardle, J. F. C. & Kronberg, P. P., 1974. *Astrophys. J.*, **194,** 249.
Wilson, A. S., Samarasinha, N. H. & Hogg, D. E., 1985. In: *The Crab Nebula and Related Supernova Remnants*, p. 133, eds Kafatos, M. C. & Henry, R. B. C., Cambridge University Press.